PAPER Special Section on Recent Progress in Antennas and Propagation in Conjunction with Main Topics of ISAP2012

Sandbank and Oyster Farm Monitoring with Multi-Temporal Polarimetric SAR Data Using Four-Component Scattering Power Decomposition

Tzu-Yu CHENG[†a)], ***Nonmember***, **Yoshio YAMAGUCHI**[††], ***Fellow***, **Kun-Shan CHEN**[†], **Jong-Sen LEE**[†], ***and*** **Yi CUI**[††], ***Nonmembers***

SUMMARY In this paper, a multi-temporal analysis of polarimetric synthetic aperture radar (Pol-SAR) data over the sandbank and oyster farm area is presented. Specifically, a four-component scattering model, being able to identify single bounce, double bounce, volume, and helix scattering power contributions, has been employed to retrieve information. Decomposition results of a time series RADARSAT Pol-SAR images acquired over the western Taiwan coast indicate that the coastal tide level plays a key role in the sandbank and oyster farm monitoring. At high tide levels, the underlying sandbank creates a shallow area with an increased roughness of the above sea surface, leading to an enhanced surface scattering power as compared to the ambient water. Contrarily, at low tide levels, the exposed sandbank appears to be a smooth scatterer, generating decreased backscattering power than the surrounding area. On the other hand, the double-bounce scattering power is shown to be highly correlated with the tide level in the oyster farms due to their vertical structures. This also demonstrates a promising potential of the four-component scattering power decomposition for coastal tide level monitoring applications.

key words: *four-component decomposition, polarimetric synthetic aperture radar (Pol-SAR), radar polarimetry, coherency matrix*

1. Introduction

Sandbank, or sandbar, typically formed at the river mouth in the sea, plays an important role to reduce the coast erosion by ocean waves. Because of its shielding capability, the area between the sandbank and the coast is often an excellent candidate for sea farming or aquaculture [1]. Monitoring of the sandbank is, therefore, very important for the ecosystem and fishery economics of coastal or island countries.

In situ investigation of the sandbank area is generally difficult, costly, and even dangerous. Not only limited amounted of data can be obtained by manual sampling, the shallow area also imposes hazard on watercrafts. Alternatively, remote sensing techniques provide an effective and safe tool for nonintrusive large spatial coverage measurement. Synthetic aperture radar (SAR), in particular, is one promising means due to its advantages in all-time/all weather operational capability and wide-area surveillance. Recent state-of-the-art SAR systems such as the RADARSAT-2 and AlOS-PALSAR are also equipped with fully polarimetric data-take capability which is able to provide much more target information than that of single-polarization SAR.

The motivation of this paper is then to provide a multi-temporal analysis of the sandbank area using polarimetric SAR (Pol-SAR) images. The area under study is the Waisanting sandbank, the largest sandbank of Taiwan. A time series of RADARSAT-2 Pol-SAR imagery data have been acquired during 2009/03/15 to 2012/09/07 for continuous monitoring. The Waisanting sandbank presents two distinctive terrains. One is a large sandbank that is mainly consists of the sedimentary deposit from the flushing river. The other is an oyster farm that is built about the sandbank containing dense vertical structures. More importantly, both of these two targets will be regularly submerged or exposed due to different sea/tide levels which play a key role in changing the backscattering behaviors for the incident waves. In order to reveal such a change, among the many analyzing tools for Pol-SAR data [2]–[8], in this paper we have adopted the model-based four-component scattering power decomposition [4], [7] because of its ability to distinguish different scattering mechanisms. To our best knowledge, this is the first study dedicated to observe the unique dynamic responses of both the sandbank and surrounding oyster farm simultaneously.

It should be noted that an earlier work [8] has been also done for polarimetric analysis of oyster farm using L-band AIRSAR data. However, the study is conducted on a single-temporal Pol-SAR dataset due to the irregularity of the AIRSAR mission. Multi-temporal analysis is performed based on JERS-1 single-channel intensity images. On the other hand, the multi-temporal analysis given in this paper is based on fully polarimetric time series Pol-SAR data. Using model-based decomposition, this allows us to extract the most indicative scattering mechanism with respect to environmental change. For example, we will show (in Sect. 3) that the double-bounce scattering power is highly correlated with the sea/tide level in the oyster farms due to the existence of vertical structures thereof.

This paper is organized as follows. In Sect. 2, the four-component scattering power decomposition with polarization orientation angle compensation [3], [7] is introduced. In Sect. 3 the experimental results of applying the four-component on the time series RADARSAT-2 Pol-SAR im-

Manuscript received January 21, 2013.
Manuscript revised May 16, 2013.
[†]The authors are with NCU, Taoyuan-sei, 320 Taiwan.
[††]The authors are with Niigata University, Niigata-shi, 950-2181 Japan.
a) E-mail: chenzina67@gmail.com
DOI: 10.1587/transcom.E96.B.2573

ages are given. The change of scattering mechanisms with respect to sea/tide levels in both sandbank and oyster farm is also analyzed in Sect. 3. Finally, Sect. 4 concludes this paper.

2. Methodology

For self-completeness, in this section, we briefly summarize the modified four-component scattering power decomposition with rotation compensation that is recently proposed by Yamaguchi et al. [7]. Pol-SAR measures the scattering matrix [S]. In the horizontal (H) and vertical (V) polarization basis, the scattering matrix can be expressed as

$$[S(HV)] = \begin{bmatrix} S_{HH} & S_{HV} \\ S_{VH} & S_{VV} \end{bmatrix} \tag{1}$$

Once the scattering matrices are obtained, we further define the coherency matrix, which retains the second order statistics of the corresponding polarimetric information. Specifically, denote $<\ >$ the ensemble average, then the coherency matrix is given by

$$\langle [T] \rangle = \left\langle k_p k_p^{\dagger} \right\rangle = \begin{bmatrix} T_{11} & T_{12} & T_{13} \\ T_{21} & T_{22} & T_{23} \\ T_{31} & T_{32} & T_{33} \end{bmatrix} \tag{2}$$

where $\dagger$ denotes complex conjugation and transposition, and the Pauli vector k_P is defined as

$$k_p = \frac{1}{\sqrt{2}} \begin{bmatrix} S_{HH} + S_{VV} \\ S_{HH} - S_{VV} \\ 2S_{HV} \end{bmatrix} \tag{3}$$

It should be noted that the ensemble averaged coherency matrix contains 9 independent parameters whereas the scattering matrix contains 5 independent parameters.

Based on the coherency matrix, many scattering power decomposition techniques have been proposed [6], [7]. The methodology we have adopted in this paper for polarimetric analysis is the four-component scattering power decomposition with rotation of coherency matrix (Y4R) [7] because it takes target orientation as well as non-reflection symmetry into account and has been proved to give reasonable results across various types of terrains.

In general, the four-component scattering power decomposition scheme is illustrated in Fig. 1. According to the different physical scattering natures, the measured coherency matrix is expanded with a library of four mechanisms, i.e., the surface scattering, the double bounce scattering, the volume scattering, and the helix scattering [6].

The expansion matrix for the surface scattering is

$$[\mathrm{T}]_{surface} = \begin{bmatrix} 1 & \beta^* & 0 \\ \beta & |\beta|^2 & 0 \\ 0 & 0 & 0 \end{bmatrix}, |\beta| < 1 \tag{4}$$

The double bounce scattering matrix can be written as

$$[\mathrm{T}]_{double} = \begin{bmatrix} |\alpha|^2 & \alpha & 0 \\ \alpha^* & 1 & 0 \\ 0 & 0 & 0 \end{bmatrix}, |\alpha| < 1 \tag{5}$$

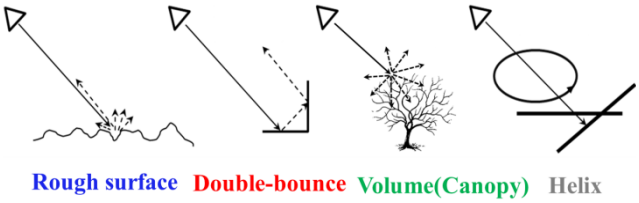

Fig. 1 The four-component decomposition by scattering natures.

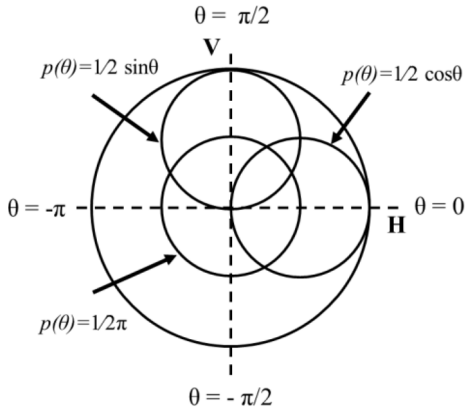

Fig. 2 Probability density function of the orientation angle. The angle θ is taken from the horizontal direction seen from the radar line of sight.

where α and β are unknowns to be determined.

The volume scattering is often assumed to be generated by a cloud of dipoles which emulates the random scattering from vegetation. If the orientation angles of the dipoles are uniformly distributed, the corresponding coherency matrix for the volume scattering is given as

$$\langle [T] \rangle_{vol} = \frac{1}{4} \begin{bmatrix} 2 & 0 & 0 \\ 0 & 1 & 0 \\ 0 & 0 & 1 \end{bmatrix} \text{ for } p(\theta) = \frac{1}{2\pi} \tag{6}$$

where $p(\theta)$ represents the probability density function of the orientation angles. When $p(\theta)$ [4], [6] has a different form other than uniform distribution as shown in Fig. 2, the volume scattering model will be modified accordingly as follows.

$$\langle [T] \rangle_{vol}^{dipole} = \frac{1}{30} \begin{bmatrix} 15 & 5 & 0 \\ 5 & 7 & 0 \\ 0 & 0 & 8 \end{bmatrix} \text{ for } p(\theta) = \frac{1}{2} \cos\theta \tag{7}$$

$$\langle [T] \rangle_{vol}^{dipole} = \frac{1}{30} \begin{bmatrix} 15 & -5 & 0 \\ -5 & 7 & 0 \\ 0 & 0 & 8 \end{bmatrix} \text{ for } p(\theta) = \frac{1}{2} \sin\theta \tag{8}$$

Selecting the appropriate volume scattering models can be based on the value of $10\log(|S_{vv}|^2/|S_{hh}|^2)$ as shown in Fig. 3.

Finally, the helix scattering accounting for the non-reflection symmetry terms is represented by

$$\langle [T] \rangle_{helix} = \frac{1}{2} \begin{bmatrix} 0 & 0 & 0 \\ 0 & 1 & \pm j \\ 0 & \mp j & 1 \end{bmatrix} \tag{9}$$

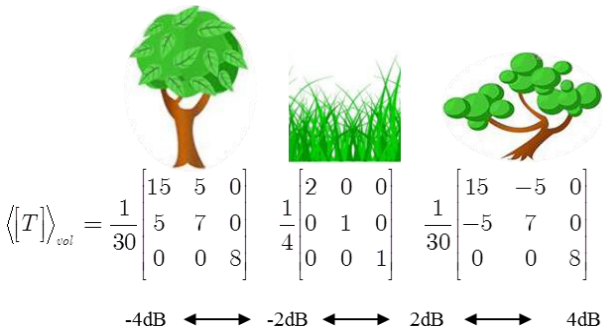

Fig. 3 The volume scattering model selection based on $10\log(|S_{vv}|^2/|S_{hh}|^2)$.

Using the four-component scattering models given in (4)–(9), we can expand the measured coherency matrix into four sub-matrices representing different scattering mechanisms. However, in order to take target orientation effect in to account, the measured coherency matrix is first rotated by an angle θ around the radar line of sight [7].

$$\langle [T(\theta)] \rangle = [R_P(\theta)] \langle [T] \rangle [R_P(\theta)]^{\dagger} \tag{10}$$

where the rotation matrix and orientation angles are respectively given by:

$$[R_P(\theta)] = \begin{bmatrix} 1 & 0 & 0 \\ 0 & \cos 2\theta & \sin 2\theta \\ 0 & -\sin 2\theta & \cos 2\theta \end{bmatrix} \tag{11}$$

$$2\theta = \frac{1}{2}\tan^{-1}\left(\frac{2\mathrm{Re}(T_{23})}{T_{22}-T_{33}}\right)$$

Consequently, the expansion coefficients (scattering powers) as well as the unknown model parameters can be derived by matching the expansion matrices to (10) as follows

$$\langle [T(\theta)] \rangle = f_s \langle [T] \rangle_{surface} + f_d \langle [T] \rangle_{double} + f_v \langle [T] \rangle_{vol} + f_c \langle [T] \rangle_{helix} \tag{12}$$

Conventionally, the decomposition result is often displayed in a pseudo-color coded image with red denoting the double-bounce scattering power, green for the volume scattering power, blue for the surface scattering power, and yellow for the helix scattering power.

3. Experimental Results

3.1 Data Information

The time series Pol-SAR data were acquired by the Canadian satellite RADARSAT-2 that is equipped with a fully polarimetric data-take mode in the C-band [5]. During 2009/03/15–2012/09/07, it has observed the Waisanting sandbank (the largest sandbank in Taiwan located in 23.00N, 123.00E) with the quad-pol mode for 9 times as listed in Table 1. Figure 4 displays the fathogram (recorded by a sonic depth finder) of the study area, which indicates the

Table 1 Time series RADARSAT-2 fully polarimetric SAR data.

No	Date	Tidal	Wind speed
1	2009/04/08	-0.72m	12.6 m/s
2	2009/05/26	-1.71m	7.9 m/s
3	2009/06/19	0.90m	1.4 m/s
4	2009/08/06	-1.12m	6.7 m/s
5	2009/08/30	0.91m	8.3 m/s
6	2012/06/03	-0.71m	12.4 m/s
7	2012/07/21	-1.23m	6.2 m/s
8	2012/08/14	0.14m	5.4 m/s
9	2012/09/07	0.62m	1.4 m/s

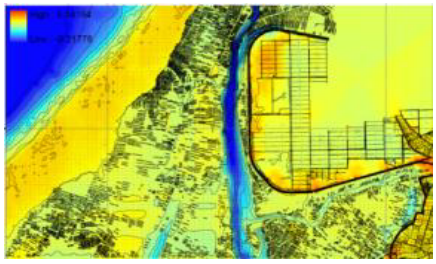

Fig. 4 Fathogram of the Waisanting sandbank. The image covers 430 m × 277 m area.

Fig. 5 The Waisanting sandbank and surrounding oyster farm.

underwater topography near the sandbank. Figure 5 shows the on-site survey photos. It can be seen that in addition to the sandbank, oyster farms are also built in the surrounding area with vertical poles standing above the shallow sea surface. The simulated dynamics of the tidal level is depicted in Fig. 6 in which the white area represents the exposed underwater sandbar. The simulation shows that the exposed area of the sandbar as well as the oyster farm is increasing when the tidal level is decreasing. The red rectangular in Fig. 6 constitutes the selected test area in this study.

The tidal level changes from time to time. Figure 7 shows the tidal levels of different dates in an ascending order, which will be used in later analysis in Sect. 3.2.

3.2 Decomposition Results

In order to obtain consistent results, the 9 Pol-SAR images are all projected to the common geodetic system (WGS84) and followed by the improved sigma filter [9] with 9×9 processing windows to obtain the estimate of coherency matrix. Figure 8 displays the decomposition results of the multi-temporal Pol-SAR data after implementation of Y4R. For

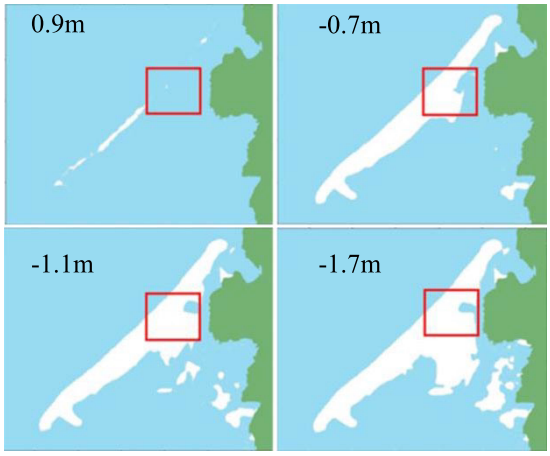

Fig. 6 Tidal level simulation.

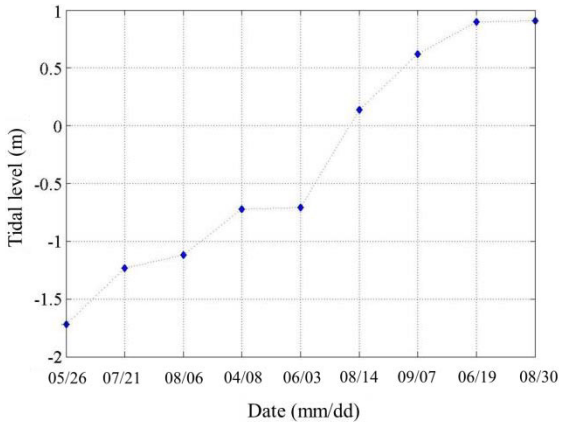

Fig. 7 Tidal level of different dates when the data were taken.

the purpose of straightforward interpretation, the images are also arranged with respect to the ascending order of the tidal level instead of acquisition date. As previously mentioned, the colors respectively represent: red for the double bounce power, blue for the surface scattering power, and green for the volume scattering power.

In each image of Fig. 8, the middle region is the sandbank. The blue color demonstrates that the main scattering mechanism is surface scattering (HH and VV polarizations are in phase). This is consistent with the fact that the sandy ground mainly consists of bare surfaces. However, Fig. 8 shows that the decomposition results of the sandbank appear differently with respect to the tidal levels. When the tidal level is low, most of the sandbank is exposed in the air and appears very dark (black color) as shown in Figs. 8(a)–(e). It indicates that the sandbank surface is a very smooth scatterer for the incident wavelength (6 cm). Instead, the sea wave nearby the sandbank (shallow sea wave) causes strong surface scattering. When the tidal level becomes high (more than −100 cm), the sandbank surface will be partially or completely buried under the sea and exhibits the surface scattering nature as shown in Figs. 8(f)–(i). The underlying sandbank creates a shallow area which increases the roughness of the above sea surface. Consequently, an enhanced surface scattering power as compared to its ambient water can be seen. Another interesting phenomenon is that the sea area in Fig. 8(d) and Fig. 8(e) has higher surface scattering power than other images. This is because of that these two day have the largest wind speed as shown in Table 1 (No. 1 and No. 6). The wind speed will affect the ocean wave roughness and hence the backscattering powers.

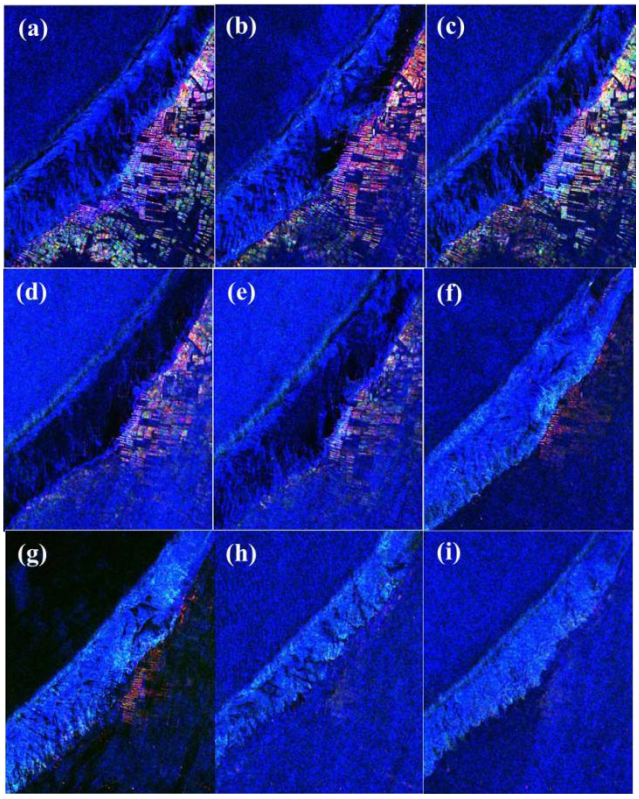

Fig. 8 Four-component decomposition images of RADARSAT-2 data. Each image contains 1000 × 800 pixels. The pixel spacing in the slant range and azimuth directions are 5.4 m and 7.9 m, respectively.

The area on the right side of the sandbank in Fig. 8 is the oyster farm. It can be seen from the upper-left image (lowest tidal level) to the bottom-right (highest tidal level) that red color in the oyster farm decreases and blue color begins to dominate. The strength of the red color represents the double-bounce scattering (HH and VV polarizations are out of phase) power coming from the oyster farm area and is the strongest for the lowest tidal level. This means that the double-bounce scattering is caused by the dihedral structures formed between the sea surface and the vertical poles above it. If the tidal is low, the emerged portion of the vertical poles becomes large with respect to the wavelength (6 cm as in C-band) so that the effective area of the dihedral structure increases, resulting in strong double-bounce scattering powers. On the other hand, if the tidal level is high, more of the vertical poles will be submerged, so that the effective area of the dihedral structure becomes small, leading to decreased double-bounce scattering powers. It is seen in Fig. 8(i) that the double-bounce scattering power

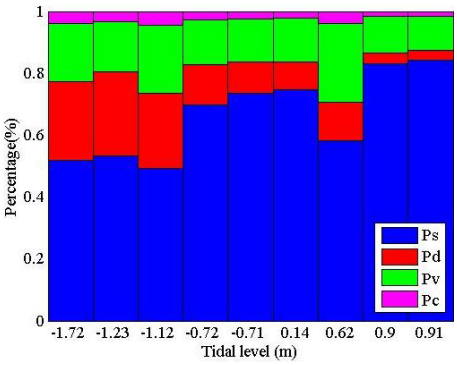

Fig. 9 Scattering power distributions in the sandbank area of the time-series Pol-SAR data.

almost disappears for the tide level of 0.9 m.

The power contribution of the decomposition for each date is displayed in Fig. 9. From left to right, the tidal level increases. It can be seen that the surface scattering is the main scattering mechanism (more than 70% for most of the dates). However, the double-bounce scattering caused by oyster farm has a clear decreasing tendency depending on the tidal level. This situation can be related to simulation as shown in Fig. 6, where the land surface is displayed as a function of tidal level. However, it should be noted that the Fig. 9 only reflects the relative percentage of different components but not their absolute values. Special notice goes to the date of 2012/09/07 when the tide level is around 0.62 m. The wind speed on that day is the lowest according to Table 1 and so the surface scattering from the sea surface is rather weak as can be seen from Fig. 9. Consequently, the relative percentage of double-bounce component appears to increase while its absolute power has indeed decreased as will be illustrated in Fig. 10.

In order to quantitatively investigate the effect of tidal level on the polarimetric decomposition powers, the scatter plot of the decomposition powers (in dB) against the tidal levels is drawn in Fig. 10(a). For comparison purposes, the scatter plots of the polarization powers in the linear and Pauli basis are also shown in Fig. 10(b) and Fig. 10(c), respectively. It can be seen in Fig. 10 that the double-bounce scattering power P_d that is extracted from the four-component decomposition has the steepest slope in the regression line with the widest dynamic range. This indicates that the double-bounce scattering power is the most sensitive with respect to the change of tidal levels. Furthermore, the correlation coefficients between the tidal level and different polarimetric powers are calculated and listed in Table 2. As is consistent with the observation in Fig. 10, the correlation coefficient is highest for the double-bounce scattering power among others. Therefore, the double-bounce scattering power can be used as a good estimator for tidal level change monitoring in the oyster farms.

4. Conclusion

In this paper, an application of the four-component scat-

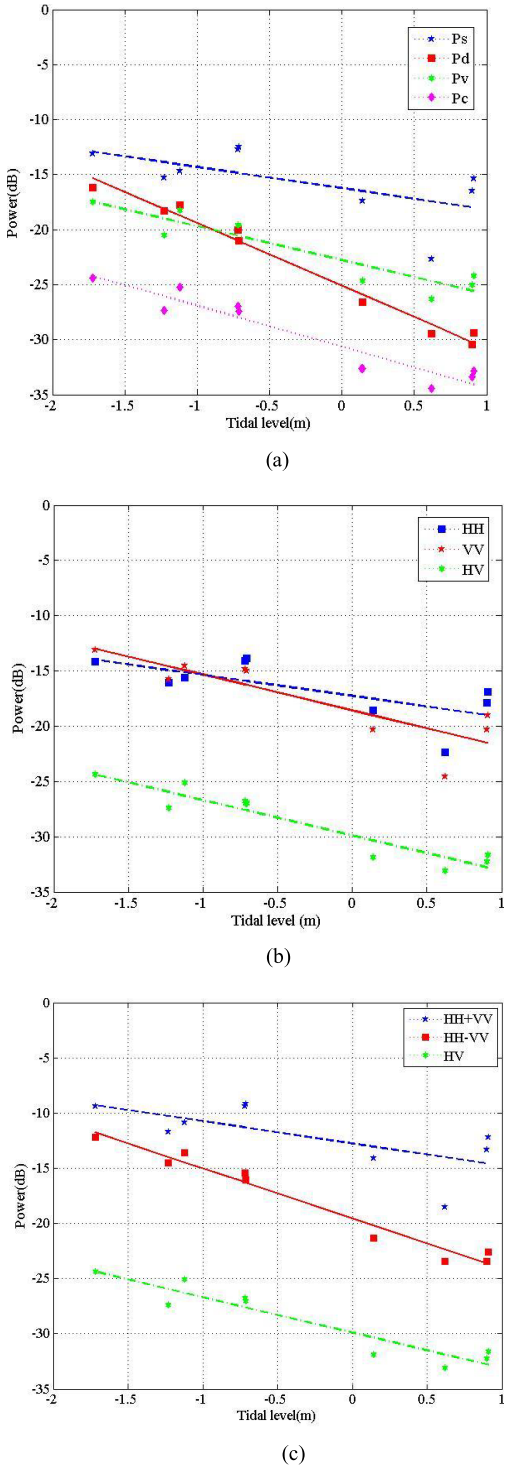

Fig. 10 Polarimetric powers as a function of tidal level. (a) Four-component powers (b) HV-basis powers (c) Pauli-basis.

Table 2 Correlation coefficient of each method.

Four-comp.	HV-basis	Pauli-basis
P_d (-0.8801)	HH (-0.7600)	HH-VV (-0.8741)
P_s (-0.5415)	VV (-0.6136)	HH+VV (-0.5934)
P_v (-0.8256)	HV (-0.8380)	HV (-0.8380)
P_c (-0.8490)	X	X

tering power decomposition on multi-temporal analysis of time series Pol-SAR datasets for sandbank and oyster farm monitoring has been presented. It has been seen that the C-band RADARSAT-2 data can be effectively used for observing the change of scattering mechanisms. In particular, we have shown that the sea/tide level plays a key role in altering the backscattering scattering behaviors from both the sandbar and oyster farms. The result also validates the necessity and effectiveness of the newly developed model-based techniques as well as their potentials for quantitative applications.

Acknowledgement

The authors would like to thank the editors and anonymous reviewers for their invaluable comments to improve the presentation of this paper.

References

[1] C.Y. Chu, T.Z. Cheng, H.W. Wang, K.S. Chen, Y. Yamaguchi, and J.S. Lee, "Sandbar analysis of polarimetric SAR image using four-component scattering decomposition," Electronic Proc. ISAP 2012, 1C4-2, Oct. 2012.
[2] Y. Yamaguchi, Radar Polarimetry from Basis to Applications, IEICE, Japan, 2007.
[3] J.S. Lee and E. Pottier, Polarimetric Radar Imaging From Basics to Applications, CRC Press, 2009.
[4] A. Freeman and S.L. Durden, "A three-component scattering model for polarimetric SAR data," IEEE Trans. Geosci. Remote Sens., vol.36, no.3, pp.963–973, 1998.
[5] Online available: http://www.asc-csa.gc.ca/eng/satellites/radarsat-2/
[6] Y. Yamaguchi, T. Moriyama, M. Ishido, and H. Yamada, "Four-component scattering model for polarimetric SAR image decomposition," IEEE Trans. Geosci. Remote Sens., vol.43, no.8, pp.1699–1706, 2005.
[7] Y. Yamaguchi, A. Sato, W.M. Boerner, R. Sato, and H. Yamada, "Four-component scattering power decomposition with rotation of coherency matrix," IEEE Trans. Geosci. Remote Sens., vol.49, no.6, pp.2251–2258, June 2011.
[8] S.K. Lee, S.H. Hong, S.W. Kim, Y. Yamaguchi, and J.S. Won, "Polarimetric features of oyster farm observed by AIRSAR and JERS-1," IEEE Trans. Geosci. Remote Sens., vol.44, pp.2728–2735, 2006.
[9] J.S. Lee, T.L. Ainsworth, and K.S. Chen, "Speckle filtering of dual-polarization and polarimetric SAR data based on improved sigma filter," Proc. IGARSS, 2008.

Tzu-Yu Cheng received the M.E. degrees in Remote Sensing Science and Technology from National Central University, Taiwan, in 2012. She is now a doctoral student in the same university and currently studying under the double degree program at Niigata University, Japan. She has been engaged in polarimetric synthetic aperture radar image analysis.

Yoshio Yamaguchi received the B.E. degree in electronics engineering from Niigata University, Niigata, Japan, in 1976 and the M.E. and Dr. Eng. degrees from Tokyo Institute of Technology, Tokyo, Japan, in 1978 and 1983, respectively. In 1978, he joined the Faculty of Engineering, Niigata University. From 1988 to 1989, he was a Research Associate at the University of Illinois at Chicago, USA. His interests are in the field of radar polarimetry, microwave sensing, and imaging. Dr. Yamaguchi has served as Chair of International Union of Radio Science Commission F Japanese Committee (URSI-F) Japan (2006–2011), and Technical Program Committee Co-Chair of the 2011 IEEE International Geoscience and Remote Sensing Symposium. He is Fellow of IEEE and a recipient of the 2008 IEEE GRSS Education Award.

Kun-Shan Chen received the Ph.D. degree in electrical engineering from the University of Texas at Arlington, Arlington, TX, USA, in 1990. Since 1992, he has been with the faculty of the Center for Space and Remote Sensing Research at the National Central University. He served as Director from 2001 to 2004 and currently holds a remote sensing Chair Professorship since 2008. He has been Director of the Communication System Research Center at the same university. He was awarded a distinguished visiting Chair Professorship from the National United University, Taiwan, in 2009 for a six-year term. He received an outstanding contribution award from Vietnam Academy of Science and Technology in 2009 for his long-term involvement of cooperative research on rupture deformation and subsidence in Vietnam. He has authored and co-authored over 100 referred journal papers, contributed five book chapters, and is coauthor of "Microwave Scattering and Emission Models for Users" (Artech House, 2010). His research interests include image processing and analysis of remote sensing data, remote sensing for natural hazards and disasters, and microwave scattering and emission theory and modeling from terrain with applications to environmental watch and resource investigation, and wireless communications. Dr. Chen was a Guest Editor for the IEEE TRANSACTIONS ON GEOSCIENCE AND REMOTE SENSING "Special Issue on Remote Sensing for Major Disaster Prevention, Monitoring and Assessment" (2007), Guest Editor for the PROCEEDINGS OF THE IEEE "Special Issue on Remote Sensing for Natural Disaster" (2012), a founding Chair of the Geoscience and Remote Sensing Society (GRSS) Taipei Chapter, an Associate Editor of the IEEE TRANSACTIONS ON GEOSCIENCE AND REMOTE SENSING (2000–2011), Deputy Editor-in-Chief of IEEE JOURNAL OF SELECTED TOPICS IN APPLIED EARTH OBSERVATIONS AND REMOTE SENSING (2008–2010), in which he also is an Associate Editor. He has been actively involved in establishing a GRSS link to Asia and Southeast Asia, in lines of natural disasters monitoring by remote sensing. He was a recipient of the distinguished award of the National Science Council 2012.

Jong-Sen Lee received the A.M. and Ph.D. degrees from Harvard University, Cambridge, MA, USA, in 1965 and 1969, respectively. After graduation, he joined the U.S. Naval Research Laboratory (NRL), Washington, DC, USA. After 37 years of service, he retired in 2006 as the Head of the Image Science Section, Remote Sensing Division. Since 2006, he has been a consultant at NRL and a Visiting Professor at the Center for Space and Remote Sensing Research, National Central University, Chung-Li, Taiwan. His professional expertise encompasses synthetic aperture radar (SAR) and polarimetric SAR (PolSAR) information processing including radar polarimetry, PolSAR speckle statistics, speckle filtering, supervised and unsupervised PolSAR terrain and land-use classification, digital image processing, radiative transfer, and control theory. He has contributed toward the pertinent current state of the arts and has published 80 journal papers, six book chapters, more than 200 conference proceedings, and a textbook (jointly with Prof. E. Pottier) entitled Polarimetric Radar Imaging: From Basics to Applications (Taylor and Francis (CRC), 2009). Dr. Lee was the recipient of the 2009 Distinguished Achievement Award of the IEEE Geoscience and Remote Sensing Society. He is a Life Fellow of IEEE for his contribution toward information processing of SAR and PolSAR imagery. He was presented the Best Paper Award (jointly with E. Pottier) and the Best Poster Award (jointly with D. Schuler) at EUSAR2000 and EUSAR2002, respectively. He was an Associate Editor of the IEEE TRANSACTIONS ON GEOSCIENCE AND REMOTE SENSING.

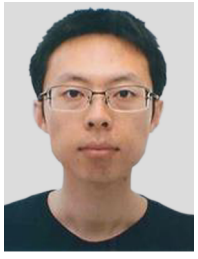

Yi Cui received the B.S. degree (with honors) in electronic information science and technology from Jilin University, Changchun, China, in 2006 and the Ph.D. degree in information and communication engineering from the Tsinghua University, Beijing, China, in 2011. From August 2011 to March 2013, he was a postdoctoral fellow with Niigata University (Japan) where he is now an assistant professor. His research interests include SAR image processing, radar polarimetry, and electromagnetic theory. Dr. Cui is the first-prize winner of the student paper competition at the 2010 Asia-Pacific Radio Science Conference (AP-RASC'10), and a recipient of the best paper award of the 2012 International Symposium on Antennas and Propagation (ISAP'2012).